

## Optimizing diffusive surface topology through a performance-based design approach

Louena SHTREPI<sup>1</sup>; Tomás MÉNDEZ ECHENAGUCIA<sup>2</sup>; Elena BADINO<sup>1</sup>; Arianna ASTOLFI<sup>1</sup>

<sup>1</sup> Politecnico di Torino, Italy

<sup>2</sup> ETH Zürich, Switzerland

### ABSTRACT

Different numerical techniques have been used in the last decades for the acoustic characterization and performance optimization of diffusive surfaces. However, these methods require advanced theoretical knowledge, very long calculation times and do not give an immediate feedback. Therefore, these methods result highly difficult to be applied by designers at an early stage of the design process, when successive design iterations are necessary from an aesthetic point of view. A suitable alternative could be the use of parametric modelling in combination with performance investigations during the design process. To this aim, this study presents a design process for diffusive surfaces optimization based on the combination of parametric models and geometrical acoustic simulations. It aims to provide architects and designers with rapid visual and acoustic feedback at a preliminary stage of their design. The process has been tested on different case studies, which have been modelled based on geometric guidelines for diffusive surface optimization. The sensitivity of the method showed that it could be a very useful tool for comparisons between design alternatives. Finally, the advantages and limitations of the integrated optimization in comparison with conventional optimizations are discussed.

Keywords: Simulations, Scattering, Diffusion

### 1. INTRODUCTION

Different theoretical models have been used to analyse the sound waves reflected by a diffusive surface (1-4). Usually they are implemented based on finite element (FEM), boundary element (BEM) and finite difference time domain (FDTD) methods, which require advanced theoretical knowledge, long calculation times and hardly present an immediate feedback. Due to these aspects, designers and architects are left apart from the acoustical investigation of the surfaces they design. Therefore, it is likely that their aesthetic preference will prevail on the optimal acoustic performance. Although it is more than a decade that the standard ISO 17497 (5, 6) has proposed the scattering and diffusion coefficients measurements, further work is needed in order to increase designers' awareness on diffusive surface design through simple design rules and approaches that could lead to an optimized result in architecture.

Acoustic performance has been considered as a key design factor of the built environment, however only recently it has been included among the optimization criteria for architecture and design (7). Integrated parametric design tools and geometric acoustic based software could reduce the required efforts by designers to obtain useful feedback in the conceptual stages of the design workflow (8-10). Moreover, this integrated approach can be helpful in the manufacturing process. The advancement of the production technologies has made possible the generation of very complex surfaces. Examples of the use of 3D printers, CNC milling machines, and industrial robots can be found in recent studies (10-13). The design affordances of acoustically efficient patterns for sound scattering has been investigated by Reinhardt et al. (13) through computational design and prototyping based on robotic fabrication. Rapid prototyping has been used also by Peters and Olesen (10) for an easier fabrication of scattering surfaces samples with hexagonal elements as primitive geometries with varied depth and width. The data obtained by measurements according to ISO 17497-1 (5) method was used to inform the parametric design tools for the performance optimization. Further, visionary explorations based on a process of architectural and acoustic tuning (7) suggest the deployment of robots to evaluate the designs of diffusive surfaces and directly react on the measured results during the fabrication

<sup>1</sup> louena.shtrepi@polito.it; elena.badino@polito.it; arianna.astolfi@polito.it

<sup>2</sup> mendez@arch.ethz.ch

process by modifying the surface shape. A detailed analysis and comparison of the design processes of these works has been introduced in Shtrepi (14). It shows that all the presented case studies imply a workflow that includes development of computational design tools, geometry generation, fabrication of prototypes as test surfaces, measurement of the acoustic performance, and the integration of these data into a generative tool (10-13). At the moment, this approach requires a customization of existing software through computer-programming (15) and requires designers to think programmatically and have programming skills (16). The success of the integrated approaches will lead to new professional figures that would embrace design and acoustic knowledge in order to generate valid solutions from both aesthetic and acoustic point of view with less effort.

This research presents a method for diffusive surfaces optimization based on the integration of parametric models and geometrical acoustic simulations. A 3D modelling software (Rhinceros) integrated to a parametric design tool (Grasshopper) and a geometrical acoustic based on ray tracing method (RT) have been used to optimize and test the performance of complex diffusive surfaces. The main aim of this study is to provide architects and designers with a tool that could give rapid visual and acoustic feedback at a preliminary stage of their design.

## 2. Methods

The analysis of the diffusive properties of fourteen surfaces has been presented in two parts. In the first part, four simple 1D diffusers have been tested using a BEM method (Reflex AFMG) and the results have been used to assess the performance of the proposed ray tracing (RT) method. In the second part, the design process of ten 3D diffusive surface has been reported showing the enhancement of the performance at each geometrical variation (5 steps).

The optimization considers the coefficient proposed by ISO 17497-1:2004 (5), which refers to the measurement of the random-incidence scattering coefficient in diffuse field, and ISO 17947-2:2012 (6), which refers to the measurement of the directional diffusion coefficient in free-field. The scattering coefficient is defined as the ratio of the non-specularly reflected sound energy to the total reflected energy. The diffusion coefficient is intended to be a measure of quality of the diffusers, i.e. a measure of the uniformity of the scattered sound. Both these coefficients are frequency dependent single numbers.

Therefore, the optimization aims towards 1) a maximization of the scattered energy with respect to the specularly reflected energy, i.e. a random-incidence scattering coefficient close to 1, and 2) a more uniform polar distribution of the scattered energy for any source angles, i.e. a diffusion coefficient value close to 1. The first parameter has not been assessed with a direct method in this work, as the amount of non-specularly reflected energy was assumed to increase on the basis of geometric rules applied to optimize the diffusive performances of the surfaces (14, 17). The focus of the optimization process has been put on the optimization of the second parameter, i.e. diffusion coefficient, with the aim to promote a more uniform spatial distribution of the reflected sound energy.

### 2.1 Optimization process

In the optimization process two approaches have been followed; a qualitative and a quantitative analyses. It should be noted that both approaches are based on ray tracing (RT) assumptions as they do not consider the wave equations and treat the sample as perfectly rigid and without any absorptive properties. Therefore, no frequency dependence is considered.

In the qualitative analyses, a visual inspection of the 3D polar distribution of the reflected rays and a comparison with a target distribution that represents a uniform spatial distribution over a hemisphere are performed. The virtual scene is shown in Figure 1-a. In this process, the rays are generated by an omnidirectional sound source located at 10m from the surface sample ( $\approx 10\text{m}^2$ ), which is positioned horizontally. The sound source can be moved at different azimuth ( $\phi$ ) and elevation angles ( $\theta$ ). All the reflected rays are stopped over a boundary hemisphere of radius 5m after being reflected by the surface sample. It is possible to visualize the reflection path length (m) and running time (ms) for each reflection.

In the second phase, an objective function optimization has been considered based on the normalized sound pressure levels over two orthogonal semi-circles. In this case the set up follows the indications of the standard ISO 17497-2 (6). The virtual scene is shown in Figure 1-b. The diffusion coefficient is estimated using the ray tracing (RT) acoustic simulations in a virtual anechoic room. The sample ( $\approx 10\text{m}^2$ ) is positioned horizontally while the sound source location can be chosen by the user. In this paper, it is located in different positions along two orthogonal semi-circles with a radius of 10m. A series of receivers are distributed over two orthogonal semi-circles with a radius of 5m that surround the panel. The equal spacing of the spherical receivers along the orthogonal semi-circles, as well as their radius, are directly related with the objective of capturing all of the energy being reflected from the sample in the direction of the semi-circles. The radius of the receivers is equal to the spacing between them, meaning that the centre of a given receiver is tangent to

the sphere of the neighbour receiver.

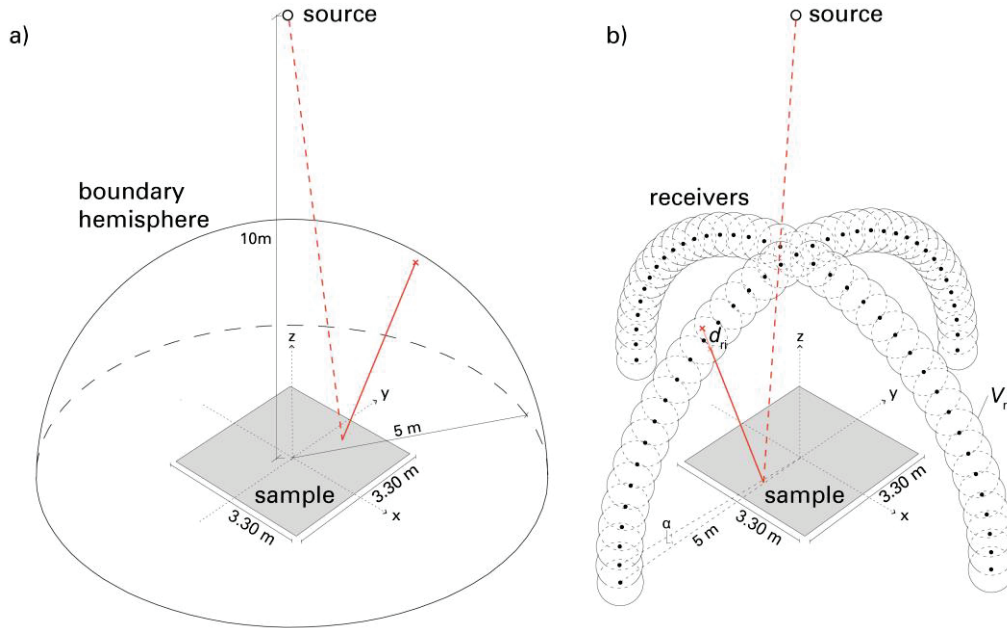


Figure 1 – Virtual scene used in the acoustic simulations for the a) qualitative and b) quantitative analyses.

The acoustic simulations performed to estimate the reflected sound energy at each receiver position are based on the raytracing method (RT), as outlined by Xiangyang et al. (18). The sound source is defined as an omnidirectional source with a sound power  $W_0$ . Since the simulations are intended to estimate the performance of a small panel, and in the interest of reducing calculation times, the sound source shoots sound rays uniformly in the solid angle towards the panel. This study does not consider the sound absorption of the panel, nor the attenuation caused by the air, therefore, the sound power contained by each one of the sound rays is:

$$W_i = \frac{W_0}{N} \quad (1)$$

where  $N$  is the number of sound rays. The  $i_{th}$  ray is considered to cross a given spherical receiver  $r$ , if the shortest distance from the ray to the centre of the receiver  $d_c$  is smaller than the receiver radius.

The sound intensity contributed to the receiver  $r$  by the  $i_{th}$  ray is defined as:

$$I_i = \frac{W_i d_{ri}}{V_r} \quad (2)$$

where  $V_r$  is the receiver volume, and  $d_{ri}$  is the distance travelled by the  $i_{th}$  ray inside of the  $r$  receiver:

$$d_{ri} = 2 \cdot \sqrt{r_r^2 - d_c^2} \quad (3)$$

where  $r_r$  is the receiver radius.

When a ray goes through the centre of a receiver, all of its energy is recorded in the receiver itself, and none of it is given to its neighbour as the distance ( $d_{ri}$ ) travelled by the  $i_{th}$  ray inside the neighbour receiver will be equal to zero as shown in equations 2 and 3. In this case, the  $i_{th}$  ray is tangent to the neighbour receiver sphere. If the ray passes through a location in between two receivers, then the energy is shared between them with proportion to their  $d_{ri}$  values. For example, a ray passing exactly through the middle of two receivers A and B, will have  $d_{ri}$  values for A and B equal to half their radius. According to equation 2, the intensity inside each receiver will be the result of half of the ray energy. In this way, there is never duplication or loss of energy.

Having computed the energy contributed by all sound rays to a given receiver, and assuming a sound impedance of the medium  $\rho c$  to be 400 (kg / m<sup>2</sup>s) the Sound Pressure Level ( $L_i$ ) can be calculated as:

$$L_i = 120 + 10 \log_{10} \left( \int_0^{\infty} I(t) dt \right) \quad (4)$$

These simulations lead to a visual representation of the  $L_i$  values over the two orthogonal semi-circles of receivers (xz and yz planes). The reflected energy has been represented in vectors with colour and length assigned according to the amount of reflected energy (Figure 2 and 3).

Moreover, a single value diffusion coefficient has been evaluated based on ISO 17497-2. The estimated

parameter in this phase is the diffusion coefficient defined as follows:

$$d_{\theta} = \frac{\left(\sum_{i=1}^n \mathbf{10}^{\frac{L_i}{10}}\right)^2 - \sum_{i=1}^n \left(\mathbf{10}^{\frac{L_i}{10}}\right)^2}{(n-1) \sum_{i=1}^n \left(\mathbf{10}^{\frac{L_i}{10}}\right)^2} \quad (5)$$

where  $d_{\theta}$  is the diffusion coefficient for the  $j$ -th one-third octave band considered,  $L_i$  is the sound pressure level of the reflected sound for the  $j$ -th one-third octave band considered at the  $i$ -th measurement position, and  $n$  is the number of measurement positions. Since the simulations performed here are based on ray tracing and do not consider the wave phenomena and assumes the sample as perfectly rigid without any absorptive properties, the  $d_{\theta}$  is calculated as a single number uniformity index  $u_{\theta}$  without any frequency dependence. Moreover, it should be noted that in these simulations it has not been necessary to normalize the uniformity index in comparison to a flat surface which aims to remove edge diffraction scattering effects due to the limit size of the sample under analysis. The edge diffraction scattering effects due to the limit size of the sample and any scattering property of the surfaces have not been implemented. Therefore, Eq. 5 reports directly the uniformity of scattered energy from the surface topology only.

It is assumed that the validity of the results and comparisons presented here regards only frequencies above the effective frequency  $f_0$ , which is the frequency where the scattering coefficient is maximized based on the size of the scattering elements. This feature is the first design aspect that can be controlled. The simple equation presented in (19), that is  $f_0=c/2a$  or  $f_0=c/2h$ , shows a linear relation between the frequency and the size ( $a$ =width or length, and  $h$ =height) of the scattering elements and provides the frequency at which scattering becomes effective; for higher frequencies the single faces of the irregularities reflect in a specular mode. Therefore, the simplification made by using a single number uniformity index  $u_{\theta}$  is accepted based on the main aim of this work, which is that of having besides the visual feedback also a quantitative number that allows to easily compare different design alternatives.

## 2.2 Assumptions and comparison to BEM simulations

The quantitative method has been first compared to BEM simulation performed through Reflex AFMG. It is a two-dimensional acoustics simulation software that models the reflection, diffusion, and scattering properties of a sound wave incident upon a defined geometrical structure, i.e. the method can be applied only to single plane diffusers (1D). Some assumptions are made in these evaluations, namely that the geometry extends infinitely in the third dimension. The surface of the sample is assumed to be perfectly rigid and 100% reflective. The calculation of the scattering coefficients is based on the ISO 17497-1 (5), while the  $L_i$  directivities are evaluated based ISO 17497-2 method (6). A receiver angular spacing ( $\alpha$ ), i.e. resolution of  $1^{\circ}$  has been used.

Three 1D diffusive and one flat surface have been simulated in Reflex and with the quantitative method presented in this paper. The three diffusive surfaces have a rectangular, curved and sawtooth profile with  $a=0.30\text{m}$  and  $h=0.20\text{m}$  ( $f_0=567\text{Hz}$  and  $f_0=850\text{Hz}$ , i.e. within 630Hz and 800Hz third-octave bands, respectively). The comparisons were based on the polar distributions obtained in Reflex for the different third-octave bands ( $>800\text{Hz}$ ) as well as on the uniformity  $u_{\theta}$  of the  $L_i$  distribution over a semicircle of  $n$  receivers with  $\alpha=1^{\circ}$  ( $n = 361$ ). The simulations have been performed at source positions covering  $0^{\circ}$ ,  $\pm 30^{\circ}$  and  $\pm 60^{\circ}$  over the  $xz$  plane. For the flat, rectangular and curved surface only  $0^{\circ}$ ,  $+30^{\circ}$  and  $+60^{\circ}$  have been performed since they have a symmetric geometry. Three values of the number of rays  $N_r$  (10k, 50k, and 100k) have been used to test the simulation time. Table 1 shows  $u_{\theta}$  values for each simulation. It can be noticed that the  $u_{\theta}$  values do not differ significantly for the different number of rays. The larger differences could be achieved for the curved surface at  $=0^{\circ}$  and  $30^{\circ}$ . The simulation time varied from 2-3min, 5-7min and 8-11 min for 10k, 50k and 100k rays, respectively. Based on the  $u_{\theta}$  variation and simulation time differences, it was decided to use 50k rays in the subsequent paragraphs.

Table 1 – Uniformity index ( $u_{\theta}$ ) for four surfaces using  $N_r=10\text{k}$ , 50k and 100k.

Panel profile	Flat		Rectangular			Curved			Sawtooth					
	Source location													
Nr of rays ( $N_r$ )	$0^{\circ}$	$30^{\circ}$	$60^{\circ}$	$0^{\circ}$	$30^{\circ}$	$60^{\circ}$	$0^{\circ}$	$30^{\circ}$	$60^{\circ}$	$0^{\circ}$	$30^{\circ}$	$60^{\circ}$	$-30^{\circ}$	$-60^{\circ}$
10k	0.31	0.27	0.16	0.29	0.19	0.09	0.31	0.37	0.14	0.35	0.28	0.11	0.29	0.15
50k	0.31	0.27	0.16	0.30	0.19	0.10	0.45	0.44	0.15	0.35	0.28	0.11	0.34	0.20
100k	0.31	0.27	0.16	0.29	0.19	0.10	0.47	0.47	0.15	0.35	0.28	0.11	0.30	0.20

Figure 2 shows that the polar distribution of the reflected energy from each surface represents coherently the performance of the four surfaces. The polar graphs highlight with a more intense colour the lobes resulting also from the BEM polar distributions. However, it should be noted that due to the principles on which is based the generation of the reflected rays in RT, this method tends to give an overestimated value of the uniformity  $u_\theta$  compared to the  $d_\theta$  values. This is more evident for the flat surface, where is not possible to distinguish the direction of the specularly reflected energy. Despite this systematic drawback the graphs result useful for a comparative investigation among different design alternatives as it will be reported in the following paragraph.

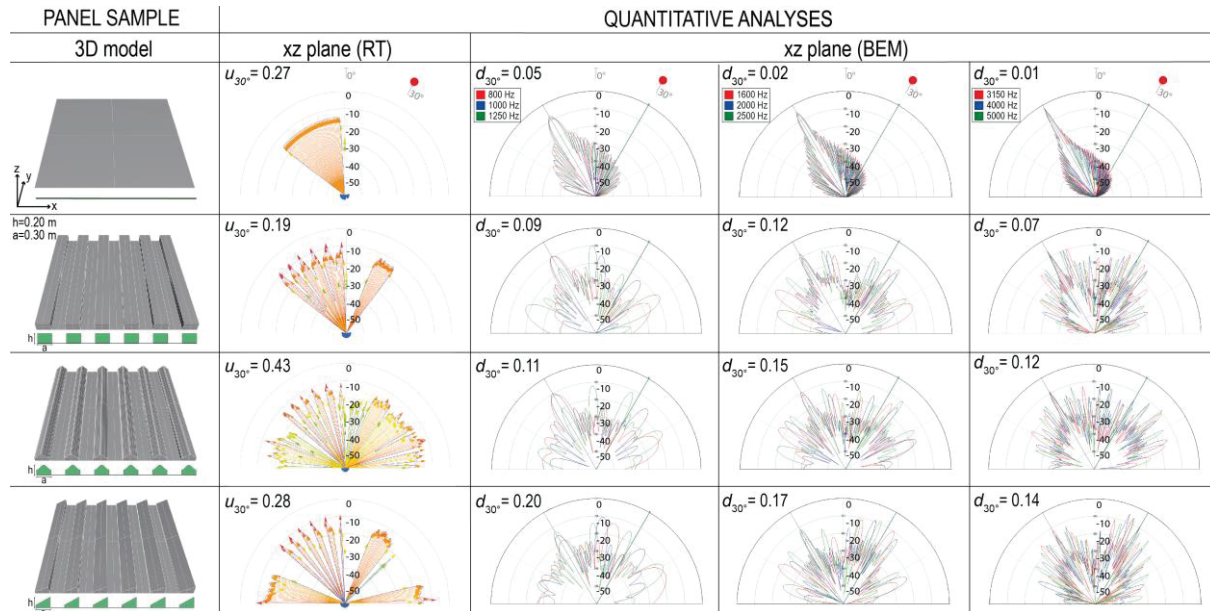


Figure 2 – Polar distribution of the reflected sound energy for source location  $\theta=30^\circ$  on the xz plane with RT and BEM method,  $d_\theta$  at 800-5000Hz third-octave bands and uniformity index ( $u_\theta$ ) for a flat and three diffusive surfaces.

### 2.3 Optimized geometries

The diffusive panels considered in the design process are squared in plan, with the length of the sides equal to 3.3 m ( $\approx 10\text{m}^2$ ). They consist of a planar base on which different arrays of elements are located, as shown in Figure 3. The process of form optimization has been structured into five steps, in which the arrangement and/or shape of these elements has been varied in the attempt to enhance the scattering and diffusion properties of the panels. The geometrical modifications applied to the panels have been selected based on the indications suggested by previous studies (20-24). The panels considered were modeled parametrically in Grasshopper for Rhinoceros, exploiting also the functionalities of the Kangaroo2 plug-in. Besides controlling the arrangement and the shape of the elements, the parametric model allowed to modify the coverage density of the elements.

As regards the arrangements of the elements, both the grid and the random distributions were tested. While, with respect to the shape variations of the elements, different forms, i.e. hexagons (as primitive elements), pyramids and truncated pyramids, as well as different dimension, i.e. different widths (0.15, 0.25, 0.30 m) and heights (0.19, 0.22, 0.25 m), were considered. Moreover, at each optimization step, two panels with different coverage densities of the elements were tested, i.e. 26-30% and 60-65%, representing low and high coverage density, respectively. Therefore, the overall number of panel configurations considered is ten, resulting from two samples with different coverage densities for each of the five optimization steps.

The starting configuration of the panel (H1) features an array of hexagonal elements (width 0.30 m, height 0.25m) arranged in a grid layout, with coverage densities of 26% and 65%. In the second optimization step, the arrangement of the elements has been randomized, to enhance the scattering properties of the panel (H2), as suggested in (20-21); the form of the elements, as well as the coverage densities were kept unaltered with respect to the previous step. As recommended in (20, 23), in the following stage, the widths and heights of the hexagonal elements (H3) have been differentiated into three options each (0.30 m, 0.25 m, 0.15 m and 0.19, 0.22, 0.25, respectively); the coverage densities tested in this phase and in the following ones are 30% and 60%. In the fourth step, the sides of the hexagonal elements have been tilted to generate pyramids (H4), which feature the same dimensions (width and height) of the previous step. This modification, in which the pyramidal elements feature facets inclined at various angles, was proposed to reflect the incident soundwaves

towards different directions and promote diffusion, as suggested in (24). To conclude, the inclination angles of the facets of the panel (H5) have been further differentiated by cutting the edges of the pyramids with randomly inclined planes to generate random pyramids (24). All these configurations have been analysed using the qualitative and quantitative approaches described in section 2.1.

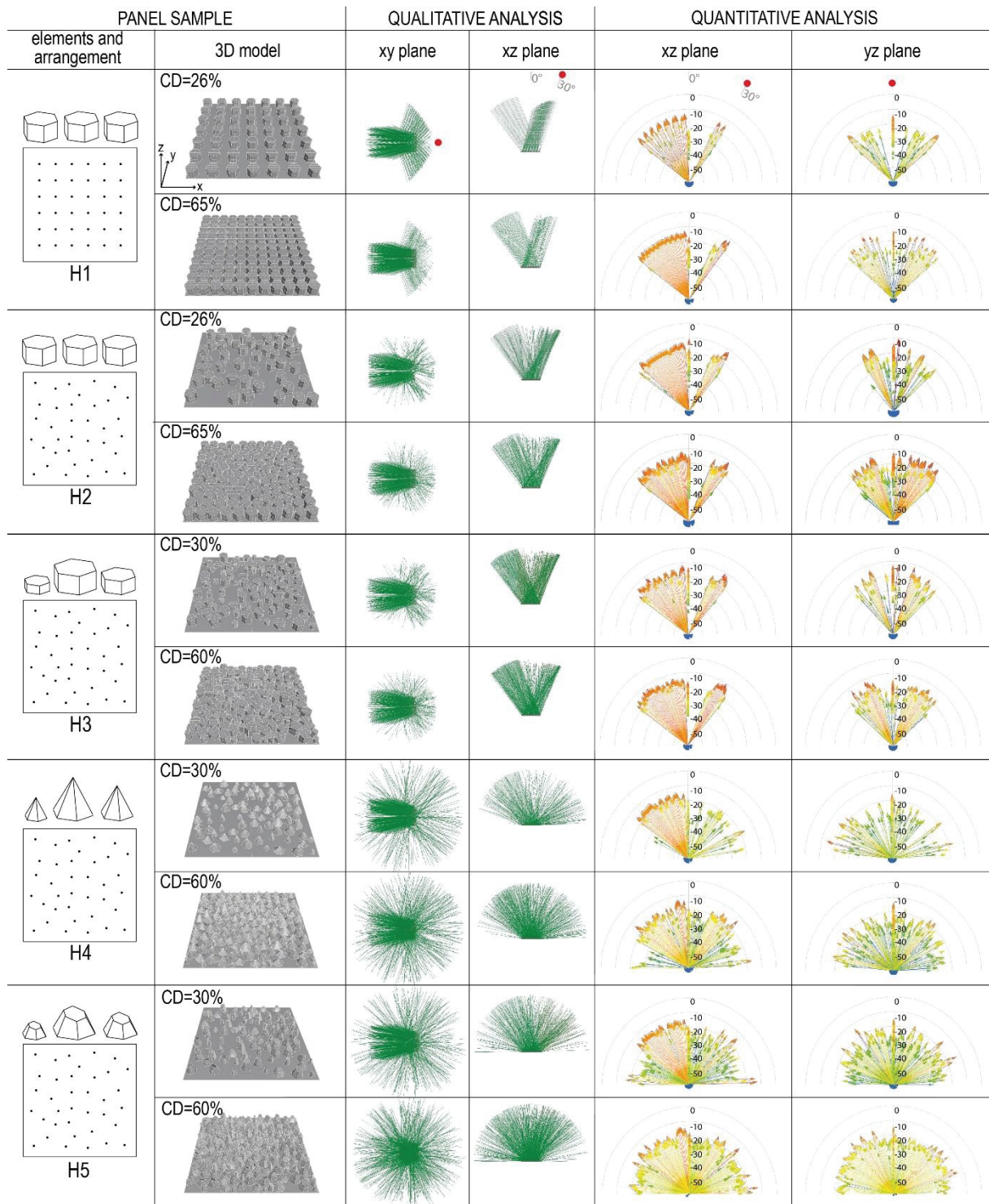


Figure 3 – Qualitative and quantitative analyses of five different optimization steps based on the arrangement and/or shape variation of the primitive elements.

### 3. RESULTS

#### 3.1 Qualitative analyses

The qualitative analysis is based on a visual inspection of the rays reflected by the sample over the

boundary hemisphere shown in Figure 1. As it has been reported above, this method can be useful for a first screening of the design alternatives.

Figure 3 shows a top and a lateral view of the optimized panels from H1 to H5. It can be noticed that panels H4 and H5 promote a more uniform distribution of the reflections and could be chosen for a further investigation based on quantitative data with more accurate methods.

### 3.2 Quantitative analyses

The quantitative analysis is based on a visual inspection of the polar distribution of the reflected energy as  $L_i$  values over two orthogonal semi-circles of receivers (xz and yz planes) and the uniformity index ( $u_\theta$ ) evaluation for the five different geometrical arrangements (H1-H5) and both coverage density values (Figure 3 and 4). Figure 3 shows the polar response (xz and yz planes) of the  $L_i$  for each panel at a source location of  $\theta=30^\circ$  on the xz plane. It can be noticed that the method is sensitive to the surface performance improvements, that is, the coverage density variations, arrangement and inclination of the faces of the primitive elements. The method seems less sensitive to the variation of the size of the primitive elements, which is expected since it mainly influences the specific frequency scattering performance, i.e. the effective frequency  $f_0$ , that is not considered in the RT implemented here. As in the previous paragraph, the polar responses highlight that it is not possible to distinguish a specific direction of the specularly reflected energy. However, it can be observed how the energy is taken off the specular zone and redirected randomly in space in the design steps from H1 to H5. In order to quantify the quality of this redirection the uniformity index  $u_\theta$  has been evaluated.

Figure 4 shows at what extent  $u_\theta$  is sensitive to the coverage density variations, arrangement, size and inclination of the faces of the primitive elements. Five sound source location have been considered at  $\theta=0^\circ$ ,  $\pm 30^\circ$  and  $\pm 60^\circ$  on the xz and yz planes. There is a slight increase of  $u_\theta$  for H1-H3 when the coverage density is increased. However, it is not significant at source locations  $\theta=\pm 60^\circ$ . H4 also shows to be sensitive to the coverage density with values of about 0.25 and 0.35 for the 30% and 60% coverage density, respectively. H5 panel outperforms the other panels leading to  $u_\theta$  values of about 0.35 and 0.50 for the 30% and 60% coverage density, respectively. It should be highlighted that real diffusers rarely reach values of diffusion coefficients higher than 0.70 (ISO 17497-2). The H5 panel shows also more similar values between the xz and yz planes. This is more evident for the lower coverage density. Therefore, the design strategies used to generate the H5 panel could be considered efficient.

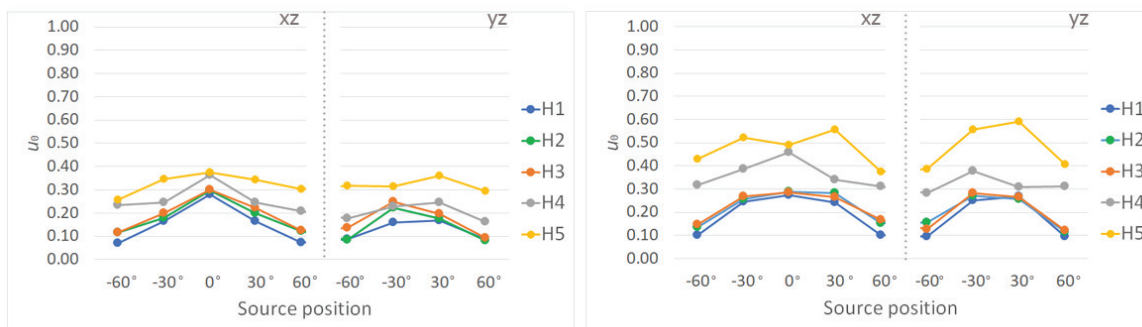


Figure 4 – The uniformity index ( $u_\theta$ ) for different locations of the source on the xz and yz planes ( $\theta=0^\circ$ ,  $\pm 30^\circ$ ,  $\pm 60^\circ$ ). evaluated for five different diffusive surfaces (H1-H5) at a coverage density of 26-30% (left) and 60-65% (right).

## 4. CONCLUSIONS

A simplified evaluating methodology of the performance of diffusive surfaces has been presented based on a qualitative and quantitative ray tracing (RT) approach. The method proposed in this work should be considered as a tool that could ease the work of the designers at the preliminary stage of the design process and that could benefit the project with less acoustic defects later. Indeed, it is helpful to get real-time feedbacks of the acoustic performance of the surface while its geometric pattern is modified. However, tests on the acceptability by architects and professionals alike should be extensively performed.

The method should be used with caution bearing in mind that the application of the RT method is limited to results at mid-high frequencies and that other wave-based phenomena such as phase, edge scattering and diffraction are not accounted. These limits led also to less sensitivity towards the size variation of the primitive scattering elements tested here. However, it was shown that the method is sensitive to the surface performance improvements related to the coverage density variations, arrangement and inclination of the faces of the primitive elements.

Further validation and improvements will be performed through comparisons with scattering and

diffusion coefficient measurements and 3D wave-based simulations.

## REFERENCES

1. Cox T. J. The optimization of profiled diffusers. *J. Acoust. Soc. Am.* 1995; 97: 2928–2936.
2. Cox T. J. Fast time domain modeling of surface scattering from reflectors and diffusers. *J. Acoust. Soc. Am.* 2015;137: EL483–EL489.
3. Redondo, J., Sánchez-Pérez, J., Blasco, X., Herrero, J. and Vorländer, M. Optimized sound diffusers based on sonic crystals using a multiobjective evolutionary algorithm. *J. Acoust. Soc. Am.* 2016; 139: 2807–2814.
4. Meyer, J., Lokki, T. Optimization of a diffuser geometry using parametric modeling tools and finite-difference time-domain simulations. *Proc. of the IOA 2018*; 4-5 October 2018; Hamburg, Germany, p.638-645.
5. ISO 17497: Acoustics -- Sound-scattering properties of surfaces -- Part 1: Measurement of the random-incidence scattering coefficient in a reverberation room, 2004.
6. ISO 17497-2:2012: Acoustics -- Sound-scattering properties of surfaces -- Part 2: Measurement of the directional diffusion coefficient in a free field, 2012.
7. Bonwetsch T., Baertschi R., Oesterle S. Adding Performance Criteria to Digital Fabrication Room-Acoustical Information of Diffuse Respondent Panels, *Proc. 28th ACADIA*, in *Silicon + Skin*, Biological Processes and Computation, Minneapolis, Minnesota 2008. p. 364-369.
8. Kolarevic B., Malkawi A.M. *Performative Architecture: Beyond Instrumentality*, Spon Press, London, 2005.
9. Peters B. Acoustic performance as a design driver: sound simulation and parametric modeling using Smartgeometry. *Int J Architect Comput* 2010; 8:337–358.
10. Peters B., Olesen T. Integrating Sound Scattering Measurements in the Design of Complex Architectural Surfaces: Informing a parametric design strategy with acoustic measurements from rapid prototype scale models, in *Future cities: 28th eCAADe Conference Proceedings*, 2010. p.481 – 491.
11. Shtrepi L., Menichelli J., Astolfi A., Mendez T., Masoero M. Improving scattering surface design with rapid feedback by integrating parametric models and acoustic simulation, *The Journal of the Acoustical Society of America* 2017; 142: 2499.
12. Kohler M., Gramazio F., and Willmann J. *The robotic touch: How robots change architecture*, Park Books, 2014.
13. Reinhardt D., Cabrera D., Jung A., Watt R., *Towards a Micro Design of Acoustic Surfaces*, in *Robotic Fabrication in Architecture, Art and Design*, Springer International Publishing Switzerland, 2016, p.137-151.
14. Shtrepi L. Advances in diffusive surface design using 3D architectural parametric modelling programs. *Proc ICA 2019*; 9 - 13 September 2019; Aachen, Germany.
15. Wortmann T., Tuncer B. Differentiating parametric design: Digital workflows in contemporary architecture and construction, *Design Studies* 2017; 52: 173-197.
16. Whitehead, H. *Laws of form*. In B. Kolarevic (Ed.), *Architecture in the digital Age: Design and manufacturing*, Taylor & Francis, 2003, p. 89-113.
17. Shtrepi L., *Diffusive surface design guidelines*, 8th Congress of the Alps Adria Acoustics Association– 21 September 2018, Zagreb, Croatia, 2018.
18. Xiangyang Z., Kean C., Jincai S. On the accuracy of the ray-tracing algorithms based on various sound receiver models, *Applied Acoustics* 2003; 64(4): 433-441.
19. Cox T. J., Dalenback B.-I., D’Antonio P., Embrechts J. J., Jeon J. Y., Mommertz E., Vorlander M., *A Tutorial on Scattering and Diffusion Coefficients for Room Acoustic Surfaces*, *Acta Acustica united with Acustica* 2006; 92: 1-15
20. Tsuchiya Y., Lee H., Sakuma T. Scale model measurements of the scattering coefficients of rib/block structure walls, *AIJ J. Technol. Des.* 2013; 19(41): 175-178.
21. Jeon J. Y., Lee S. C., Vorländer M. Development of scattering surfaces for concert halls. *Appl. Acoust.* 2004; 65(4): 341-355.
22. Shtrepi L., Astolfi A., D’Antonio G., Vannelli G., Barbato G., Mauro S., Prato A., Accuracy of the randomincidence scattering coefficient measurement, *Appl. Acoust.* 2016; 106: 23–35.
23. Lee H., Tsuchiya Y., Sakuma T. Acoustic scattering characteristics of Penrose-tiling-type diffusers, *Appl. Acoust.* 2018; 130:168–176.
24. Cox T. J., D’Antonio P. *Acoustic Absorbers and Diffusers: Theory, Design and Application*. Taylor and Francis, New York, USA, 2017.